Top-down estimate of China's black carbon emissions using surface observations: Sensitivity to observation representativeness and transport model error

JOURNAL OF GEOPHYSICAL RESEARCH: ATMOSPHERES, VOL. 118, 5781–5795, doi:10.1002/jgrd.50397, 2013

Top-down estimate of China's black carbon emissions using surface observations: Sensitivity to observation representativeness and transport model error

Xuan Wang,[1,2,3] Yuxuan Wang,[1] Jiming Hao,[2] Yutaka Kondo,[4] Martin Irwin,[4] J. William Munger,[5] and Yongjing Zhao[6]

Received 28 October 2012; revised 4 April 2013; accepted 6 April 2013; published 7 June 2013.

[1] This study examines the sensitivity of "top-down" quantification of Chinese black carbon (BC) emissions to the temporal resolution of surface observations and to the transport model error associated with the grid resolution and wet deposition. At two rural sites (Miyun in North China Plain and Chongming in Yangtze River Delta), the model-inferred emission bias based on hourly BC observations can differ by up to 41% from that based on monthly mean observations. This difference relates to the intrinsic inability of the grid-based model in simulating high pollution plumes, which often exert a larger influence on the arithmetic mean of observations at monthly time steps. Adopting the variation of BC to carbon monoxide correlation slope with precipitation as a suitable measure to evaluate the model's wet deposition, we found that wet removal of BC in the model was too weak, due in part to the model's underestimation of large precipitation events. After filtering out the observations during high pollution plumes and large precipitation events for which the transport model error should not be translated into the emission error, the inferred emission bias changed from −11% (without filtering) to −2% (with filtering) at the Miyun site, and from −22% to +1% at the Chongming site. Using surface BC observations from three more rural sites (located in Northeast, Central, and Central South China, respectively) as constraints, our top-down estimate of total BC emissions over China was 1.80 ± 0.65 Tg/yr in 2006, 0.5% lower than the bottom-up inventory of Zhang et al. (2009) but with smaller uncertainty.

Citation: Wang, X., Y. Wang, J. Hao, Y. Kondo, M. Irwin, J. W. Munger, and Y. Zhao (2013), Top-down estimate of China's black carbon emissions using surface observations: Sensitivity to observation representativeness and transport model error, *J. Geophys. Res. Atmos.*, *118*, 5781–5795, doi:10.1002/jgrd.50397.

1. Introduction

[2] Black carbon (BC) aerosol, emitted mainly from incomplete combustion of fossil fuel and biomass, is known to have adverse effects on air quality, visibility, human health, and radiation balance [*Dachs and Eisenreich*, 2000; *Jacobson*, 2001; *Ramanathan and Carmichael*, 2008]. China is regarded as the largest BC emitter in the world, contributing about 25% of the global total emissions [*Bond et al.*, 2004; *Cooke et al.*, 1999; *Ramanathan and Carmichael*, 2008]. However, bottom-up estimates of BC emissions in China, based on emission factors and statistical data of combustion activities, are subject to large uncertainties [*Bond et al.*, 2004; *Cao et al.*, 2006; *Lei et al.*, 2011; *Lu et al.*, 2011; *Qin and Xie*, 2012; *Streets et al.*, 2001, 2003a, 2003b; *Zhang et al.*, 2009]. For example, the reported uncertainty of China's bottom-up BC inventory is ±484%, ±208%, and ±98%, respectively, by *Streets et al.* [2003a], *Zhang et al.* [2009], and *Lu et al.* [2011]. The large uncertainty in the inventory data arises partly from BC emission factors which are mostly taken from those in western countries with few field measurements of combustion processes in China, and partly from the challenges of obtaining accurate activity data in China.

[3] Atmospheric measurements of BC concentrations at representative locations have provided independent "top-down" constraints on BC emissions, particularly when used in conjunction with chemical transport models or climate models that simulate the atmospheric processes of BC from

Additional supporting information may be found in the online version of this article.

[1]Ministry of Education Key Laboratory for Earth System Modeling, Center for Earth System Science, Institute for Global Change Studies, Tsinghua University, Beijing, China.
[2]School of Environment and State Key Joint Laboratory of Environment Simulation and Pollution, Tsinghua University, Beijing, China.
[3]Now at Department of Civil and Environmental Engineering, Massachusetts Institute of Technology, Cambridge, Massachusetts, USA.
[4]Department of Earth and Planetary Science, Graduate School of Science, The University of Tokyo, Tokyo, Japan.
[5]Department of Earth and Planetary Sciences and School of Engineering and Applied Sciences, Harvard University, Cambridge, Massachusetts, USA.
[6]Air Quality Research Center, University of California, Davis, California, USA.

Corresponding author: Y. X. Wang, Ministry of Education Key Laboratory for Earth System Modeling, Center for Earth System Science, Institute for Global Change Studies, Tsinghua University, Beijing, China. (yxw@tsinghua.edu.cn)

2169-897X/13/10.1002/jgrd.50397

emissions to atmospheric concentrations and deposition [*Carmichael et al*., 2003; *Hakami et al*., 2005; *Park et al*., 2005; 2010; *Hu et al*., 2009; *Koch et al*., 2009; *Fu et al*., 2012; *Kondo et al*., 2011b]. After allowing for the measurement uncertainty, one can evaluate model-calculated BC with available observations, attributing the difference to the bias in the emission inventory and/or model processes. A few studies have evaluated BC emission inventories over China using this approach, and their "top-down" estimates of Chinese BC emissions are all larger than the bottom-up estimates that are mostly based on the inventory of *Bond et al*. [2004]. *Park et al*. [2005], by comparing the modeled BC concentrations with aircraft observations during NASA Transport and Chemical Evolution over the Pacific aircraft campaign in spring 2001, suggested that the BC inventory of *Bond et al*. [2004] underestimated Chinese BC emissions by about 60%. *Koch et al*. [2009] reported that the majority of models participating in the AeroCom model intercomparison project underestimated BC surface measurements in China by more than 50%, suggesting a likely 50% underestimate of Chinese BC emissions by the inventory of *Bond et al*. [2004] and *Cofala et al*. [2007] used by the AeroCom models. Through comparison of Goddard Earth Observing System (GEOS)-Chem model results with BC measurements at 10 surface sites in China, *Fu et al*. [2012] estimated that all previous bottom-up inventories underestimated BC emissions in China by at least 60%. *Kondo et al*. [2011b] conducted a detailed modeling analysis of continuous BC measurements at a remote site (Cape Hedo) in East China Sea in combination with a chemical transport model (Community Multiscale Air Quality). They derived the total of BC emissions in China (1.92 Tg/yr) which were very close to the bottom-up inventory of *Zhang et al*. [2009] (1.81 Tg/yr).

[4] There are at least three major factors that can cause biases among the model-derived "top-down" estimates of Chinese BC emissions illustrated above: (1) the representativeness of observations employed to constrain regional-scale emissions, which depends on where the observational sites are relative to the location of emissions and whether or not the transport patterns sample randomly and uniformly across the region or have preferential paths; (2) the aggregation error of assuming uniform emission adjustments for a region instead of letting emissions be adjusted heterogeneously; and (3) the transport model error associated with grid resolution, wet deposition, and transport. The focus of this study is on the representativeness error and transport model error. Although we will briefly discuss the impact of the aggregation error, lacking a spatially comprehensive data set of BC observations prevents us from examining the aggregation error in detail.

[5] As BC measurements are scarce in China, the observations used by many of the "top-down" studies are either from short period measurements or include urban sites not suitable to represent regional characteristics. Furthermore, most studies use monthly or annual mean observations for model comparison, which can be influenced by high-concentration events more of local scale. Through statistical analysis for both measured and modeled data points, *Gilardoni et al*. [2011] pointed out that monthly or annual mean observations might not be suitable for evaluating BC modeling. *Schaap et al*. [2011] illustrated that using observational data with higher temporal resolution (hourly data) generated more accurate model evaluation for secondary inorganic aerosols. Only two studies were found to use the hourly data [*Hakami et al*., 2005; *Kondo et al*., 2011b]. *Hakami et al*. [2005] adopted hourly observations from 10 sites in Asia, within which only one site is located inside China (Yulin). However, observations from the Yulin site were not used in their top-down emission estimates, as they found this site was influenced by local sources. The top-down estimate of *Kondo et al*. [2011b] is based on hourly BC observations at a remote site (Cape Hedo) located along the East China Sea. With only one site outside China to constrain the emissions of the whole county, they conducted careful analysis using both model and observations to identify the Chinese outflows and to correct for the transport effect. Finally, previous studies did not employ the relationship between BC and other species as additional constraints. For example, the correlation between BC and carbon monoxide (CO), which has similar sources as BC but different loss processes in the atmosphere, can provide useful information on emission types and the influence of wet deposition on BC. Emission estimates of CO from China are also subject to large uncertainties. The bottom-up inventory of *Zhang et al*. [2009] estimated annual CO emissions in China to be 167 Tg in 2006 with an uncertainty of ±185%, similar to the inventory of *Street et al*. [2006]. *Zhao et al*. [2012] suggested that the interannual variations of CO emissions in China were small from 2005 to 2009, with the national total emissions around 179 Tg/yr. Using surface observations and CO retrievals from MOPITT (Measurement of Pollution in the Troposphere) satellite instrument as observational constraints, *Tanimoto et al*. [2008] derived a top-down CO emission estimate of 170 Tg for China. *Bian et al*. [2010] compared the simulated CO columns by the Goddard Global Ozone Chemistry Aerosol Radiation and Transport (GOCART) model using the inventory of *Zhang et al*. [2009] with MOPITT CO retrievals and found a difference of less than 20%. This difference was attributed not only to the anthropogenic emissions but also to biomass burning emissions and the OH levels in the model. From these studies, it seems that the bias of CO emissions in *Zhang et al*. [2009] is less than 20%. Many measurement studies have analyzed the observed relationship between BC and CO [*Andreae et al*., 2008; *Li et al*., 2007; *Pan et al*., 2011; *Wang et al*., 2011b; *Han et al*., 2009; *Verma et al*., 2011; *Zhou et al*., 2009], but fewer modeling analysis have explored these observational constraints to evaluate the model's performance in simulating wet removal of BC.

[6] To address the issues above, this study examines the sensitivity of "top-down" quantification of Chinese BC emissions to the choice of observational data. Using hourly measurements of BC and CO at two rural sites in China, we will present a detailed analysis of the model-observation comparison to filter out those data not representative of regional emissions or heavily influenced by the model's transport errors instead of by emissions. The observed BC to CO correlation and its variation with precipitation will be used to evaluate the model's wet deposition process and to quantify the bias of wet deposition simulation on BC emission estimate. By comparing top-down BC emission estimate derived from carefully selected hourly observations with that from simple monthly mean observations, we will estimate the uncertainty of top-down emissions due to observation representativeness and model transport error. Finally, with the improved uncertainty estimates, we will use monthly mean observations at

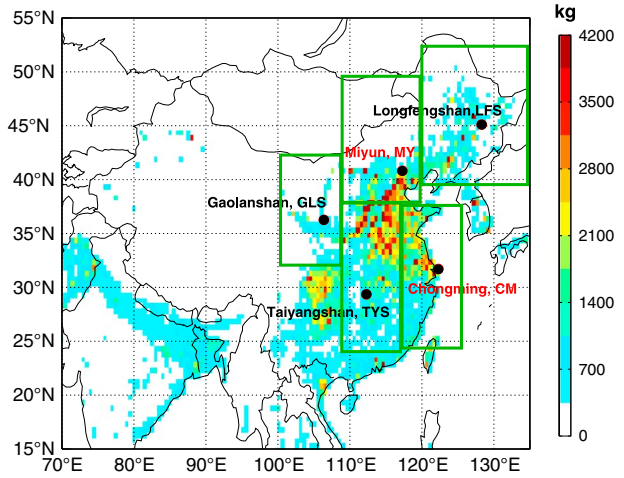

Figure 1. Locations of the five observation sites (black circles). The Miyun (MY) and Chongming (CM) sites are continuous sites with hourly observations. The color shading indicates anthropogenic BC emissions in 2006 [*Zhang et al*., 2009]. The green rectangles indicate the five regions used to evaluate China's BC emissions defined in Figure 2.

three other rural sites in China for which we do not have access to hourly observations to derive top-down BC emissions for the whole China.

2. Model and Observation Description

2.1. Model Description

[7] In this study, we used the nested-grid GEOS-Chem model [*Bey et al*., 2001; *Chen et al*., 2009; *Wang et al*., 2004] driven by meteorological data assimilated by the Goddard Earth Observing System (GEOS) at the NASA Global Modeling and Assimilation Office, version 9-1-2. The structure of the nested-grid GEOS-Chem model involves a window with a uniform horizontal resolution of $0.5° \times 0.667$ embedded in a lower resolution of $4° \times 5°$ global background. The nested-grid GEOS-Chem retains the generic high horizontal resolution of the GEOS-5 meteorological data over the nested regional domain (70°E–150°E, 11°S–55°N) which includes all of China, its neighboring countries and a significant portion of the northwestern Pacific [*Wang et al*., 2004; *Chen et al*., 2009]. The higher resolution nested-grid simulation uses lateral boundary conditions provided by the lower resolution global model that are updated every 3 h.

[8] The standard simulation of BC in GEOS-Chem mainly follows the Georgia Tech/Goddard Global Ozone Chemistry Aerosol Radiation and Transport (GOCART) model [*Chin et al*., 2002] with a few modifications. The model assumes that 80% of emitted BC are hydrophobic, which become hydrophilic with an e-folding time of 1.15 days [*Cooke et al*., 1999; *Chin et al*., 2002]. The wet removal process follows the scheme used by *Liu et al*. [2001], which includes in-cloud rainout (only for hydrophilic BC) and below-cloud washout (for hydrophilic and hydrophobic BC) for both large scale and convection precipitation. We added the correction for the fractional area distribution between in-cloud and below-cloud scavenging as implemented by *Wang et al*. [2011a]. A size-dependent parameterization of below-cloud scavenging rate proposed by *Wang et al*. [2011a] was not adopted in this work since this modification resulted in a lower correlation between modeled and observed BC at the surface sites employed here.

[9] The dry removal process is based on a standard resistance-in-series model dependent on the local surface type and meteorological conditions [*Wesely*, 1989]. For comparing with the 2010 observations at the two hourly sites (to be presented in section 2.3), the simulation is from October 2009 to December 2010, with the first 3 months as initialization. Model results for 2010 are used for analysis. For comparing with the 2006 observations at the other sites, the simulation is from October 2005 to December 2006, and the model results for 2006 are used for analyses.

2.2. BC Emission Inventories

[10] The standard GEOS-Chem simulation uses the gridded global annual BC emission inventory of *Bond et al*. [2004] for 2000 as anthropogenic BC emissions. In this study, anthropogenic BC emissions over East Asia are replaced by the newer inventory of *Zhang et al*. [2009], including both fossil fuel and biofuel emissions. The annual total of Chinese BC emission for 2006 is 1.81 Tg (±208% uncertainty, 95% confidence interval) from this inventory, which is about 33% larger than that of *Bond et al*. [2004] for emissions in 2000. The spatial correlation of the two inventories over China is 0.7. *Zhang et al*. [2009] also provided monthly variation factors of emissions, which are mainly derived from temperature differences in different seasons. We implemented the monthly variations factors for North China (north of Yangtze River) but not for South China (south of Yangtze River) as the variation of temperature and associated change in BC emissions from the residential sector are small by month in the south. Although two newer inventories are available for China [*Lu et al*., 2011; *Qin and Xie*, 2012], they are both based on the work of *Zhang et al*. [2009] with scaling factors to derive emissions for more recent years. Furthermore, unlike *Zhang et al*. [2009], these newer inventories do not include CO emissions, which are used in this study. The spatial distribution of anthropogenic

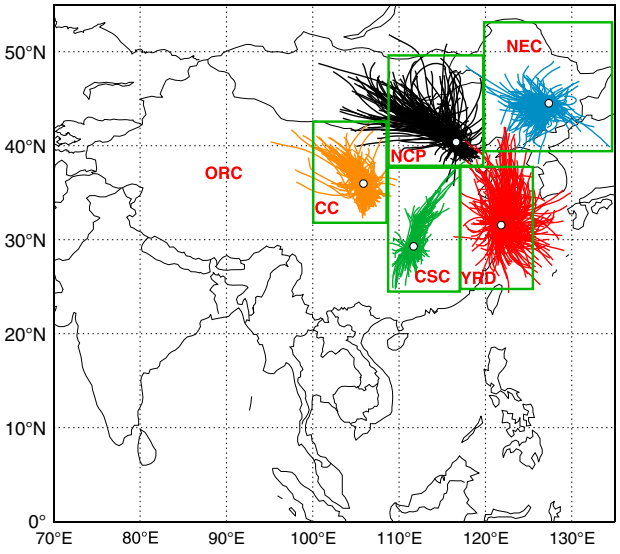

Figure 2. The 1 day back trajectories analyses for the five observation sites. The green rectangles indicate the five regions used to evaluate China's BC emissions.

Table 1. Summary of BC Measurements at the Five Selected Sites

Site	Observed Period	Sampling Frequency	Data Used	Method	BC Concentration ($\mu g/m^3$)[a]			
					Spring	Summer	Fall	Winter
Miyun	Apr–Oct 2010	1 min	Hourly mean	Optical	1.78 (1.81)	2.31 (2.37)	2.41 (2.17)	-
Chongming	Apr–Oct 2010	2 min	Hourly mean	Optical	1.11 (1.11)	1.42 (1.35)	0.86 (0.80)	-
Longfengshan[b]	2006	24 h	Monthly mean	Thermal	1.52	1.08	2.47	4.26
Taiyangshan[b]	2006	24 h	Monthly mean	Thermal	1.99	1.51	3.33	2.73
Gaolanshan[b]	2006	24 h	Monthly mean	Thermal	2.67	2.11	3.72	6.23

[a]Concentrations were 24 h averages, for Miyun and Chongming; the numbers in the brackets were daytime averages (8–18 LT).
[b]*Zhang et al*. [2008].

BC emissions over China is shown in Figure 1. BC emissions from open biomass burning are taken from the Global Fire Emission Database version 3 (GFED3) [*van der Werf et al*., 2010], which is derived using Moderate Resolution Imaging Spectroradiometer fire counts to determine the locations and periods of active fire hot spots. The GFED3 data used here has monthly resolution and covers the period from 1997 to 2010. According to the GFED3 inventory, biomass burning, even in the peak month, contributes to less than 1.5% of total BC emissions over North China Plain and Yangtze River Delta where we have hourly observations. Therefore, we did not adopt the daily resolved GFED inventory.

2.3. Observations and Region Definition

[11] Surface observations suitable to evaluate the model performance and emission inventory should be able to provide regional and seasonal information. Observations from five rural sites in China (Figure 1) are used in this study, two of which are continuous measurements of our own and the others are monthly mean observations published previously. The 1 day back trajectory analyses (Figure 2) were conducted over the whole study period for each of the five sites following the method of *Wang et al*. [2011b]. Based on the extent and density of the trajectories, we tentatively selected five regions over which observations at the five sites can represent, respectively: Northeast China (NEC), Center South China (CSC), Center China (CC), North China Plain (NCP), and Yangtze River Delta (YRD). These five regions are shown in Figures 1 and 2. Emissions from the five regions account for 78% of the national total emissions according to the inventory of *Zhang et al*. [2009]. Other regions not represented by the sites are denoted as the Other Regions of China (ORC). Compared with previous top-down studies which did not distinguish subregions within China [*Wang et al*., 2011a; *Fu et al*., 2012], the back trajectory analysis conducted here reduces the representativeness error of using only a few available sites to constrain China's total BC emissions.

[12] Our continuous observations were conducted at Miyun (MY, 40°29′N, 116°46.45′E, 152 m above sea level (asl)) and Chongming (CM, 31°31′N, 121°54′E, 24 m asl). The MY site is in a rural area located about 100 km northeast of the Beijing urban area. BC concentrations were measured every minute by the Continuous Soot Monitoring System (COSMOS, Kanomax Instruments, Japan), using an optical absorption method at a wavelength of 565 nm. BC observations at MY were discussed in detail by *Wang et al*. [2011a]. Further information about the MY site and the COSMOS instrument can be found in previous papers [*Kondo et al*., 2009, 2011a; *Miyazaki et al*., 2008; *Wang et al*., 2008, 2009, 2010] and are not repeated here. The CM site is located on the east side of the Chongming Island, about 50 km northeast of the Shanghai urban area. The site resides inside a national reserve for migratory birds, and its surroundings are mainly wetlands. BC was measured every 2 min with an Aethalometer (Magee Scientific, Berkeley, California, USA, Model AE-31). At a 590 nm wavelength channel, the results of COSMOS and Aethalometer agree quite well with a R^2 of 0.94 [*Miyazaki et al*., 2008]. Both instruments have a precision of 10%. There are no major anthropogenic sources within 20 km of either site, so observations from MY and CM can reflect regional characteristics of atmospheric BC concentrations of NCP and YRD in China, respectively. Both sites measure CO concurrently with BC, and there are also continuous measurements of SO_2, O_3, and CO_2 at MY. Due to the shallow boundary layer height and lower wind speeds unfavorable for mixing, nighttime observations may be more sensitive to local emissions. In addition, chemical transport models also perform poorly in simulating nighttime stratification of surface air [*Liu and Liang*, 2010]. Therefore, only daytime observations at the two sites are used in the analysis below. The observation period is from April to November 2010 for MY and April to October 2010 for CM. Daytime observations at the two sites during this period are summarized in Table 1.

[13] Surface observations from three other rural sites that cover other major regions in China were obtained from published papers. The three sites are Longfengshan (LFS, 44°43.8′N, 127°36′E, 331 m asl), Taiyangshan (TYS, 29°10.2′N, 111°42.6′E, 536 m asl), and Gaolanshan (GLS, 36°N, 105°51′E, 1531 m asl) (Figure 1), which provide regional characteristics of BC over NEC, CSC, and CC, respectively. The three sites belong to a carbonaceous aerosol measurement network in 2006 published by *Zhang et al*. [2008] with the observation period from January to December 2006. We selected them because they are all located at rural mountains/hills without large local sources, representing the regional conditions. The three sites were used as observational constraints for Chinese BC emissions in previous modeling studies [*Fu et al*., 2012; *Koch et al*., 2009]. BC at the three sites were measured using the thermal-chemical method every third day, so the published monthly mean data are the averages from about 10 days' observations. The location of the sites is shown in Figure 1, and the data summary is given in Table 1. Seasonal mean BC concentrations at the five sites range from 1.1 to 6.3 $\mu g/m^3$.

3. Model Evaluation

[14] Two types of model evaluation are presented in this section. First, monthly mean model results are compared

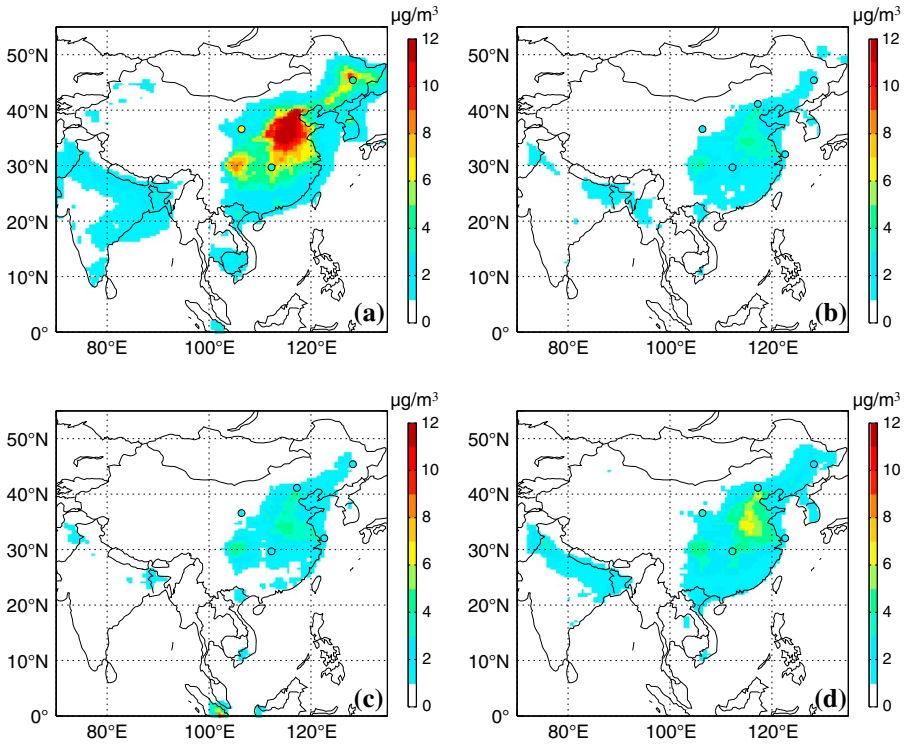

Figure 3. Spatial distribution of modeled BC in (a) January, (b) April, (c) July, and (d) October 2010, overlaid with monthly mean BC observations at the five sites (colored circles).

with monthly mean BC observations, which is the typical evaluation approach adopted in previous modeling study [*Fu et al*., 2012]. Second, hourly mean model results are compared with hourly mean observations at the two continuous sites (MY and CM) to examine if the use of higher resolution data results in different quantification of model biases. As hourly mean observations can provide more information on atmospheric processes than the monthly mean data, the former are analyzed further to examine the biases in model processes other than emissions. To ensure consistent comparison, monthly mean observations at MY and CM are derived from the same set of daytime-only hourly mean observations used for model evaluation.

3.1. Evaluation Using Monthly Observations

[15] Figure 3 shows the spatial distribution of modeled BC surface concentrations over China in January, April, July, and October 2010, overlaid with monthly mean observations at the five observation sites. BC concentrations are much higher in winter than in summer, partly due to higher emissions in winter over North China. The shallower boundary layer in winter and enhanced wet deposition in summer also explain the seasonality of BC. In terms of spatial variation, BC is higher over east China where emissions are higher than over the west, and the highest concentrations are around NCP and the Sichuan Basin. The spatial distribution of simulated BC concentrations is similar in different seasons and resembles that of the emission inventory (Figure 1) because of the relatively short lifetime of BC in the atmosphere. The model reproduces observed BC at most of the sites in spring, summer, and fall but tends to underestimate observations in winter. Modeled BC at GLS is much lower than observations in every season. Compared with *Wang et al*. [2011a] and *Fu et al*. [2012], which adopted the same observations at the three published rural sites (LFS, TYS, and GLS), the model-to-observation comparison shown in Figure 3 is consistent with their results in terms of spatial patterns, but our model results show smaller biases. Although the same inventory was used in their studies, *Wang et al*. [2011a] did not implement the monthly emission factors, whereas *Fu et al*. [2012] used one set of monthly emission factors for all of China. As stated before, we implemented the monthly variations factors only for regions north of the Yangtze River, as the variation of temperature and associated change in BC emissions from the residential sector are small by month in the south.

[16] Figure 4 compares the monthly variation of modeled and observed BC at the individual sites. The model well reproduces the mean concentrations and the month-to-month variation of BC observed at LFS (Figure 4a) and MY (Figure 4d). Although the general monthly variation is also well reproduced by the model at CM (Figure 4e), the model overestimates observed BC by about 37% before July. We found that the monthly mean wind speeds in the model were lower than observations before June, which partly explains the overestimation. The simulated BC concentrations at TYS (Figure 4b) are similar to observations except in January and February, and the model has an overall positive bias of 36% at this site. Unlike the other four sites, the model shows a large underestimation of 74% at GLS (Figure 4c).

[17] The differences between modeled and observed concentrations can be caused by biases in both emission inventories and model processes. Furthermore, the arithmetic mean of observations at monthly time steps, the most commonly reported metric of surface observations and typically adopted

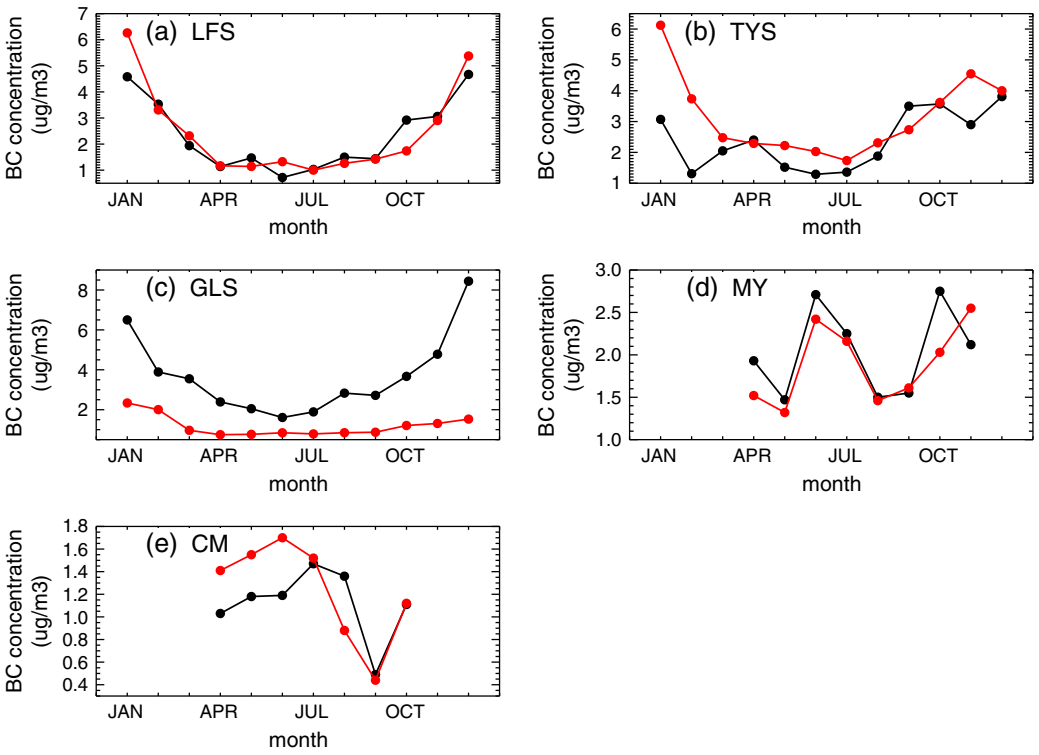

Figure 4. Monthly mean concentrations of observed (black) and modeled (red) BC at the five surface sites.

by the top-down modeling analyses, can be greatly influenced by outliers, i.e., high pollution events of episodic nature. For example, in our previous study [*Wang et al*., 2011b], we found that the high monthly mean concentration of BC observed in October 2010 at MY was caused by a 3 day pollution event in early October and did not reflect the typical observations in that month [cf. *Wang et al*., 2011a, Table 3]. This explains why the model does not reproduce the observation in October at MY (Figure 4d). The discrepancy in this case relates more to the model's transport and resolution than to the emission inventory.

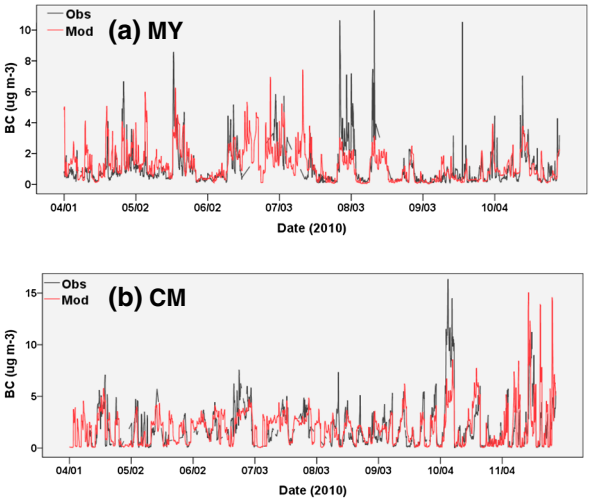

Figure 5. Hourly mean concentrations of observed (black lines) and modeled (red lines) BC at the (a) Miyun and (b) Chongming site.

The representativeness issue of monthly mean observations was not addressed in previous top-down modeling studies [*Koch et al*., 2009; *Fu et al*., 2012].

3.2. Evaluation Using Hourly Observations

[18] Figure 5 compares the time series of measured and simulated hourly BC at the MY and CM site with continuous hourly observations. Figure 6 shows the scatter plots of the comparison. The correlation coefficient square (R^2) of measured and simulated hourly BC is 0.37 and 0.36 at MY and CM, respectively. The model reproduces the temporal variation of BC at the two sites, although it underestimates many of the episodic peaks in the observation. The overall model bias is −11% and −22% against hourly observations at MY and CM, respectively, compared to that of −9% and +42% based on monthly mean observations during the same period. These biases are calculated using the same method, which is the correlation slope between modeled and observed concentrations at each site (cf. Figure 6 for hourly and Figure 11 for monthly). Because of the small number of data points for the monthly mean comparison (a maximum of 12 for a year) (Figure 11), the correlation slope and thus calculated model bias can be easily affected by 1 or 2 months of bad model performance (outliers). In contrast, hourly data provide directly point-to-point comparison at every hour and offer a much larger database for model evaluation at each site (Figure 6). Because of the large amount of data points available, individual points cannot change the overall slope significantly for the hourly case. This explains the large differences in the calculated model biases when using the same set of underlying observation data but with different temporal resolutions.

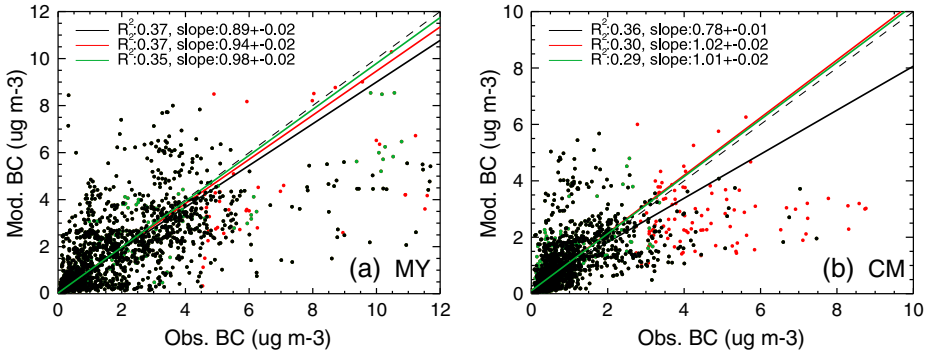

Figure 6. Modeled (y axis) versus observed (x axis) hourly mean BC concentrations at the (a) Miyun and (b) Chongming site. The correlation slope of all the data is shown by the black solid line, and the 1:1 slope is shown as a dashed black line. The pollution plumes are displayed as red dots, and the red line indicates the correlation slope after excluding these data. The green dots are the data with accumulated precipitation (AP) > 10 mm/day, and the green line indicates the slope after excluding these data. The squares of the correlation coefficient (R^2) and the correlation slope are shown inside the figure.

[19] We assume that the episodic peaks in observations are primarily caused by pollution plumes originating from occasional localized emissions or upwind urban areas. Given its spatial resolution (0.5° × 0.667°), the model is incapable of simulating transport events at the subgrid scale responsible for those peaks and tends to smear out and dilute BC concentrations of the pollution plumes within its grids. For example, as shown in Figure 5a, the model captures the episodic enhancement in BC around August 1 and 10 at MY, but it largely underestimates the observed concentrations. Similar examples can be found at CM (Figure 5b), such as around July 1 and October 7. The model's low bias in these cases relates to the intrinsic inability of a grid-based, coarse-resolution model to simulate concentrated pollution plumes and hence should not be corrected simply by scaling up regional BC emissions. Therefore, these plume events should be excluded when using the modeled-to-observed BC difference to infer a correction factor of regional BC emissions. Since the episodic pollution plumes are typically featured with simultaneous enhancements of other primary pollutants besides BC, the concurrent measurements of both BC and CO are employed to identify these pollution periods. The hourly mean observations with both BC and CO exceeding their highest 10-percentile concentration of the whole observation period are assigned as belonging to the plume cases. The 10-percentile threshold of BC is 4.5 μg/m^3 at MY and 2.7 μg/m^3 at CM, and that of CO is 1087 ppbv at MY and 753 ppbv at CM. The data points belonging to the plume cases are shown as red in Figure 7 which displays the difference between modeled and observed BC (modeled minus observed) as a function of observed BC. The plume cases identified here account for about 3% and 7% of all the data at MY and CM, respectively. As shown in Figure 7, the model underestimates most of the plume cases, providing independent evidence that these data are likely to be influenced by the pollution plumes. Sensitivity calculations are conducted by setting the threshold to the highest fifth percentile and the highest 15th percentile in order to estimate the uncertainty associated with the plume selection (to be represented later). It should be mentioned that the data points identified as the plume cases may not be all underestimated by the model. Some data in this event may even be overestimated because of model transport errors. During the plume periods, the observations are not suitable to reflect typical emission conditions regardless of the performance of the model. Exclusion of the plume cases identified based on BC and CO observations is aimed to remove as much influence from the nonrepresentative observational data as possible, rather than simply discarding those data points largely underestimated by the model.

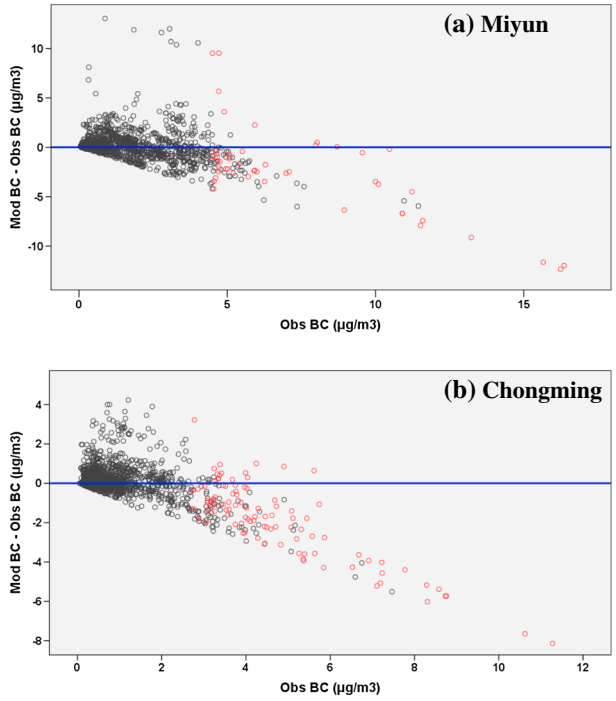

Figure 7. The differences of modeled and observed hourly BC concentrations (modeled minus observed) versus observed concentrations at the (a) Miyun and (b) Chongming site. Red circles indicate the pollution plumes.

[20] It is difficult to separately examine the model's performance on simulating different atmospheric processes of BC,

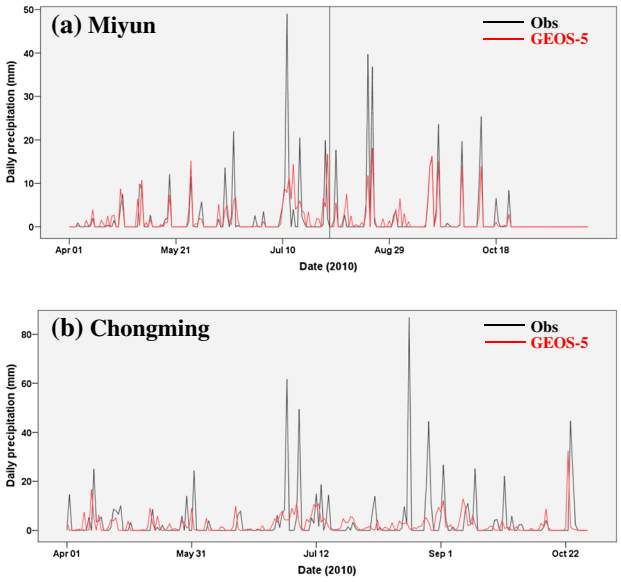

Figure 8. Comparison of observed (black) and modeled (red) daily precipitation at the (a) Miyun and (b) Chongming site. The observations are averages of several meteorological stations in proximity of the BC sites.

such as transport and dry deposition. However, as the major sink of BC, wet deposition is typically simulated using parameterization schemes relating to precipitation that can be evaluated with observed precipitation. Here we used the observed precipitation (the temporal resolution of 6 h) at meteorological stations from China National Meteorological Information Center (http://www.nmic.gov.cn/) to evaluate the precipitation field of the model. Figure 8 compares the observed daily precipitation at the meteorological station closest to MY and CM with the assimilated daily precipitation from the GEOS-5 meteorological fields for each site. The R^2 of observed and simulated daily precipitation is 0.48 at MY and only 0.1 at CM. The model does quite well when predicting rain events but underestimates the precipitation amount in the days with heavy rain. Compared to observations, the GEOS-5 assimilated precipitation has an overall underestimation of 19% and 40% at MY and CM, respectively, during the measurement period. This suggests a possible underestimation of BC's wet deposition by the model.

[21] The relationship between BC and precipitation is examined further as a possible criterion to diagnose the bias of the model's wet deposition scheme. As BC concentrations at one location are affected by wet deposition not only at the sampling location but also along the transport trajectory, precipitation data were taken from the average observation of 6 h accumulated precipitation (AP) recorded at several meteorological stations around the MY and CM site. For convenience, we converted the unit of AP from millimeters per 6 h to millimeters per day in later discussions. The observed AP for the MY site is obtained from six meteorological sites within 150 km radius of the BC measurement location (Beijing urban, Miyun, Mentougou, Gaobeidian, and Wuqing), while the observed AP for CM is taken from two meteorological sites (Baoshan and Xujiahui). We found no clear relationship between the model's discrepancy of BC and observed AP on the hourly resolution (Figure S2 in the supporting information), suggesting the confounding effects of the emission bias and transport error on diagnosing the wet deposition bias at individual hours. The measured and simulated BC concentrations were then averaged at different levels of observed AP, and the results are compared in Figure 9. The data are divided into three groups by precipitation: AP = 0, $0 < AP \leq 10$, and $AP > 10$ mm/day. Analyses using different precipitation thresholds were also conducted (results not shown), which confirms that our following analysis on the model's wet deposition bias is not sensitive to the choice of AP. The mixing ratios of CO, an insoluble tracer with similar sources as BC, are also shown in the figure. At MY (Figure 9a), observed BC and CO both show a general trend of increase with AP when $AP < 10$ mm/day, while at CM (Figure 9b), the observed BC and CO first decrease then increase with AP. As CO is affected primarily by transport, the fact that observed BC does not always decrease with increasing precipitation but exhibits similar trends as CO is an indication that transport patterns are different with different AP. As a result, the surface site may sample air masses of different source signatures when it rains or not. The model reproduces the observed change of both BC and CO with AP at MY for $AP < 10$ mm/day, but the modeled BC does not decrease as shown by the observations when precipitation is large ($AP > 10$ mm/day), suggesting that the model underestimates wet deposition of BC. The model has a poorer ability to reproduce the observed change of BC and CO with AP at CM. In contrast to observations, the simulated BC and CO both increase with AP at CM from AP = 0 to $0 < AP \leq 10$ mm/day. As CM is a coastal site, it is expected that the model cannot fully reproduce the more complicated, small-scale, land-sea circulation at CM.

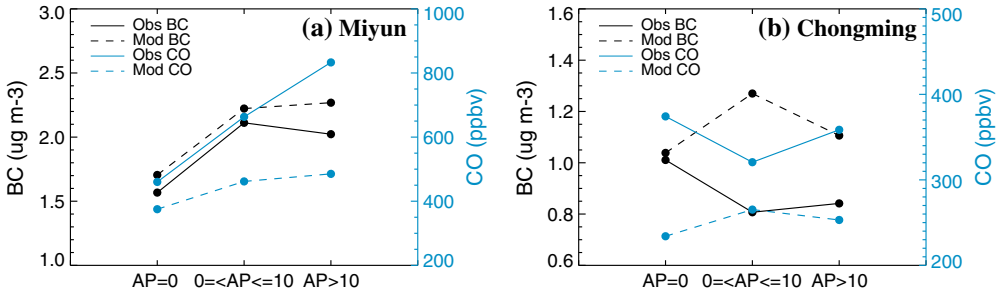

Figure 9. Variations of observed (solid lines) and modeled (dashed lines) concentrations of BC (black) and CO (blue) with different ranges of accumulative precipitation (AP) at (a) Miyun and (b) Chongming.

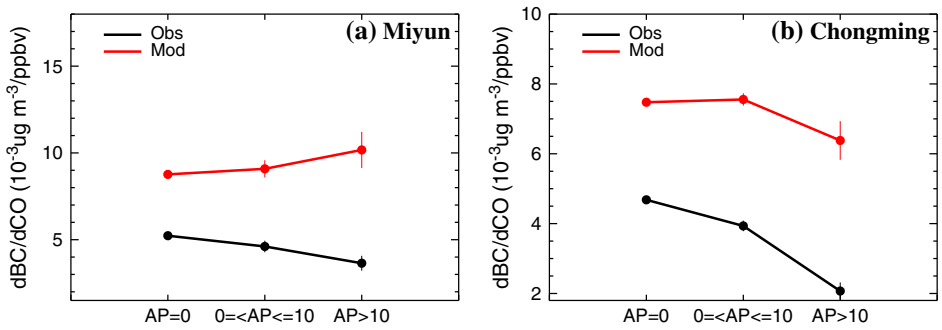

Figure 10. Observed (black) and modeled (red) BC-CO correlation slopes in different AP ranges at (a) Miyun and (b) Chongming. The BC-CO scatter plots from which the correlation slopes are derived are provided in the supporting information.

[22] Because of the influence from transport, the relationship between BC and precipitation cannot be used as a robust measure to represent the impact of wet deposition on BC. In our previous study [*Wang et al.*, 2011b], we showed that BC and CO had a strong positive correlation at MY, as their variances were affected by the same atmospheric transport and that the correlation slope between BC and CO always decreased with AP. We found the same phenomenon for BC and CO at CM. As BC and CO have similar sources and transport process, the difference is that BC is largely removed by wet deposition but CO not. Therefore, the ratio of BC to CO, in the form of BC-CO correlation slopes in the atmosphere, is expected to be lower as precipitation increases. The BC-CO correlation slopes for different AP groups are shown in Figure 10, and the BC-CO scatter plots are provided in the supporting information. The observed BC-CO slopes at MY and CM decline slightly when AP increases from 0 to 10 mm/day, and become much lower as AP exceeds 10 mm/day. The significant trend of decrease of the measured BC-CO slopes with precipitation at both sites indicates the predominant influence of wet removal on the BC-CO ratio. Therefore, the BC-CO correlation slope is a suitable measure to evaluate the model's ability of simulating wet deposition of BC based on atmospheric concentration observations.

[23] The simulated BC-CO correlation slopes at different intervals of AP are also shown in Figure 10. The model overestimates the BC-CO correlation slopes at both sites regardless of AP. We argue that the absolute difference between the observed and simulated BC-CO correlation slope is mainly caused by errors in emissions, while the relative change of the BC-CO ratio with AP represents the wet deposition effect. The model does not capture the observed large decrease of the BC-CO correlation slope from light precipitation ($0 < AP \leq 10$ mm/day) to larger precipitation ($AP > 10$ mm/day) at both sites. In contrast to observations, the simulated BC-CO slope at MY shows an increase, indicating that the wet removal process of BC in the model is too weak compared to that inferred from observations. It is difficult to provide a quantitative estimate of how much the model has underestimated wet deposition in this study because the model's transport error likely also contributes to the discrepancy between the observed and simulated BC-CO correlation slopes, and we cannot separately estimate the two types of errors. The counterfactual increase of BC-CO ratio from small precipitation ($AP < 1$ mm/day) to large precipitation ($AP > 10$ mm/day) at MY predicted by the model is likely caused by the model's transport error. The impact of transport on the BC-CO ratio depends on the upwind source regions. As shown by the back trajectories in Figure 2, the MY site samples two major types of air masses, which were referred to as the Siberian air mass group (northern air mass) and the NCP air mass group (southern air mass), respectively, in our prior paper [*Wang et al.*, 2011b]. We found that the mean BC-CO ratio for the southern air mass group was a factor of 2 larger than that for the northern air mass group [*Wang et al.*, 2011b]. As the model fails to simulate the precipitation well, this indicates the model may not simulate well the transport transition between north and south air masses during precipitation events, causing the BC-CO ratio to increase during precipitation. As we cannot provide a quantification of the wet deposition bias, a simple approach is to exclude the data during large precipitation events (AP 10 mm/day) from the analysis of emission estimation.

[24] The model's bias in simulating wet deposition of BC can be attributed to problems in simulating precipitation, BC aging process, in-cloud, and below-cloud wet removal. We showed above that the amount of precipitation predicted by the GEOS-5 assimilated meteorology was lower than that observed at the two sites. The aging process of BC is closely connected with in-cloud wet removal but is not as strongly connected to below-cloud removal, which scavenges BC regardless of its hygroscopicity. The GEOS-Chem model assumes that 80% of emitted BC is hydrophobic which become hydrophilic in a constant e-folding time of 1.15 days (27.6 h). This timescale varies from 24 h to 39 h in different models [*Koch et al.*, 2009; *Park et al.*, 2003]. Some models also parameterize BC's aging process as a function of oxidants (i.e., O_3 and OH), the mixing state of aerosols, and meteorological conditions [*Croft et al.*, 2005; *Huang et al.*, 2012; *Koch et al.*, 2009; *Liu et al.*, 2011]. We conducted a sensitivity simulation in which all the emitted BC were hydrophilic. The simulated BC-CO correlation slope reduced by 5% in the case of large precipitation (AP thinsp;> 10 mm/day), far from sufficient to correct for the overestimation shown in Figure 10. Although both in-cloud and below-cloud wet removal are connected with precipitation, in-cloud scavenging has a weaker dependence on the amount of ground precipitation than below-cloud scavenging does. In-cloud wet scavenging

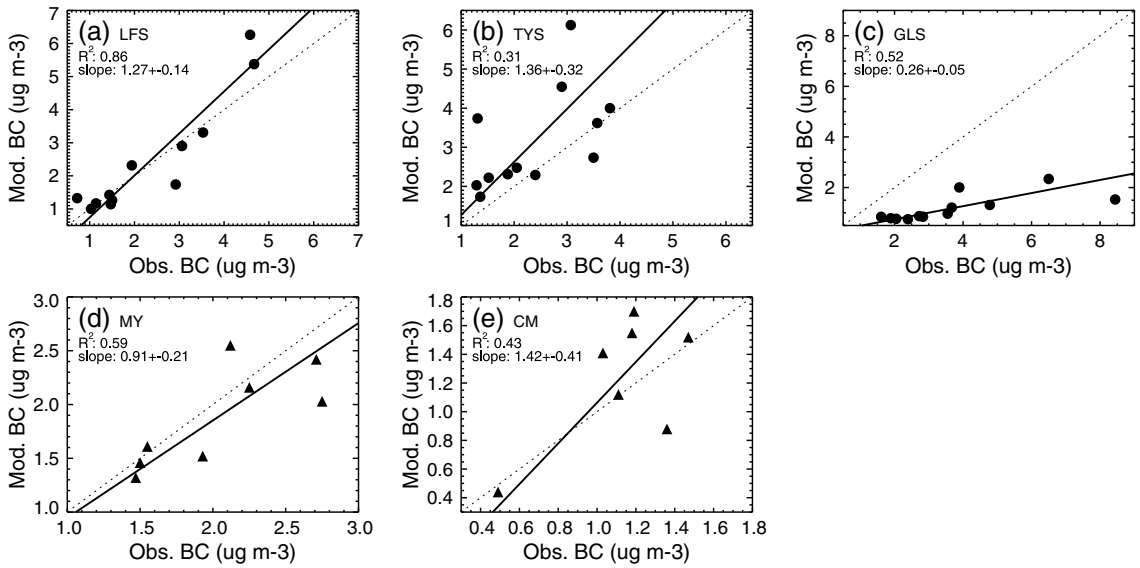

Figure 11. Modeled versus observed monthly mean BC concentrations at the five sites. The dashed black line is the 1:1 line, and the correlation slope is shown as the solid black line. The squares of the correlation coefficient (R^2) and slope are shown in each plot. (a, b, and c) Circles represent the 24 h mean data at the monthly mean sites, and (d and e) triangles are daytime mean data at the MY and CM site where we have hourly observations.

is determined by precipitation at the upper levels, rather than by ground precipitation examined here. In contrast, below-cloud scavenging at the surface level is determined by ground precipitation and can affect surface BC as soon as rain occurs. Therefore, given that the model's bias is largest when ground precipitation is largest, we speculate that the model bias is more likely to be associated with below-cloud than with in-cloud wet removal. Our argument here is different from that of *Feng* [2007] and *Wang et al.* [2011a]. They suggested that the below-cloud wet removal scheme of *Liu et al.* [2001] overestimated BC scavenging because it did not consider aerosol sizes. The addition of aerosol size distribution in below-cloud scavenging scheme of the GEOS-Chem model proposed by *Wang et al.* [2011a] was not adopted here, as this modification would result in an increase of model biases when compared with MY and CM observations. Additional observations of the vertical profile of BC are needed to investigate this issue.

4. Top-Down Emission Estimate

4.1. Influence of Different Data Use

[25] To derive the top-down constraints on BC emissions, we adopted the typical assumption used in previous studies that BC surface concentrations over China corresponded almost linearly to emission changes in China; thus, the mean difference between modeled and observed BC concentrations can be used as a scaling factor to correct for the bias of the BC emission inventory used in the model [*Kondo et al.*, 2011b; *Fu et al.*, 2012] This linearity, which was verified in our model's sensitivity simulation in which emissions were increased by 50% (Figure S3 in the supporting information), arises because of BC's relatively short lifetime and the linearity of wet removal on BC concentrations. The mean difference between modeled and observed surface concentrations are derived from their correlation slopes of the reduced-major-axis regression that treats the two variables as symmetrical (Figure 11) [*Hirsch and Gilroy*, 1984]. We first examine the extent to which the top-down emission estimation can vary when different observational data are used as constraints: monthly observations, hourly observations, and hourly observations after the exclusion of the pollution cases and wet deposition influence.

[26] We first use the monthly mean BC concentrations at the five rural sites as observational constraints, and the emission evaluation results are shown in Table 2. For example, the correlation slope between observed (x axis) and modeled (y axis) monthly mean BC at LFS (Figure 11a) is 1.27, suggesting that

Table 2. The Emission Bias Derived at the Individual Sites Using Different Observational Data

Site[a]	LFS	TYS	GLS	MY	CM
Monthly mean data	1.27[b]±0.14[c]	1.36 ± 0.32	0.26 ± 0.05	0.91 ± 0.21	1.42 ± 0.41
Hourly mean data	-	-	-	0.89 ± 0.02	0.78 ± 0.01
After excluding the plume cases	-	-	-	0.94 ± 0.02	1.02 ± 0.02
After excluding both the plume cases and AP > 1 mm points	-	-	-	0.98 ± 0.02	1.01 ± 0.02

[a]LFS = Longfengshan, TYS = Taiyangshan, GLS = Gaolanshan, MY = Miyun, CM = Chongming.
[b]Correlation slope between modeled and observed BC (Mod/Obs).
[c]Standard deviation in the derivation of correlation slopes.

the emission inventory used in the model overestimated regional BC emissions sampled at LFS by 27%. Using the monthly data as constraints, we estimated that the emission inventory had a bias of +27% at LFS, +36% at TYS, +42% at CM, −9% at MY, and −74% at GLS.

[27] As we have discussed in the previous section, using hourly mean instead of monthly mean observations can cause large differences in the magnitude of model biases. At the MY and CM site, when hourly observations were used as constraints, the bias of the emission inventory as derived from the regression correlation slope (Figure 6 and Table 2) was −11% at MY and −22% at CM. This can be compared with the emission bias of −9% at MY and +42% at CM derived before using the monthly mean observations.

[28] Although the true emissions were unknown, compared with monthly mean observations, the use of hourly mean observations as constraints can improve emission estimate in three aspects. First, hourly observations enable a direct point-to-point comparison between observation and model. With only month mean information, it is difficult to separate the impact of outliers caused by local effects (extremely high or low concentrations within 1 month) on the overall model bias. Second, the nighttime data can be excluded when hourly observations are available. The monthly mean observations at MY and CM were compiled after excluding the nighttime data because we have hourly observations at these sites. When nighttime data were not excluded at the two sites, the monthly mean concentrations showed a change of less than 10% for the observations (cf. Table 1) but increased by 60% for the model results. Therefore, this exclusion of nighttime data avoids misinterpreting the poor performance of the model in simulating nighttime boundary layer as emission biases. This exclusion cannot be done at the three other sites with only monthly mean observations. Third, when estimating annual emissions, there are only 12 monthly mean observations available at a given site to evaluate the emissions, and the results can be easily affected by one or two bad simulation months. The amount of hourly data points during the course of 1 year is large enough to represent the average condition of emission biases with statistical significance.

[29] However, not all the hourly observations at hourly time steps are representative of regional emissions. As discussed above, the model has a poor ability to correctly simulate the plume cases and large precipitation events at MY and CM. The model's deficiencies in the two cases should not be transferred to corrections for the emission inventory. Therefore, at the MY and CM sites, hourly observations after excluding the plume cases and large wet deposition influence (identified in section 3.2) are regarded as the best possible data set of observational constraints for regional emissions. The emission bias derived from the regression correlation slope (Figure 6 and Table 2) was −2% at MY and +1% at CM. Compared with the bias of −11% at MY and −22% at CM derived from the hourly observations without data exclusion, the differences are large for both regions. Removal of the pollution cases from the hourly data resulted in an increase of 5% and 24% for the emission estimates at MY and CM, respectively, and removal of the large precipitation cases made a difference of 4% and 1% for the two regions (Table 2). The two data exclusions have a much larger influence on the top-down emission estimate at CM than MY because there were relatively more data points belonging to the two cases at CM due to its coastal location and wetter climate. To estimate the uncertainties from the two exclusions, we conducted sensitivity calculations in which the threshold of the pollution cases varied from the highest fifth percentile to the highest 15th percentile, and the AP threshold for the large precipitation cases varied from 0 to 20 mm/day. The resulting uncertainty was ±2% at MY and ±13% at CM for the pollution cases and ±1% at MY and ±8% at CM for the wet deposition cases (Table 2).

[30] The 2% and 13% uncertainty for the pollution cases at MY and CM, respectively, indicates the resolution error of the $0.5^\circ \times 0.667^\circ$ resolution model used in this study. It does not represent the resolution error of the coarser resolution models used by previous studies. We conducted a $2^\circ \times 2.5^\circ$ resolution GEOS-Chem global simulation with the same emission inventory. The simulated monthly mean BC concentrations at the five sites differ by a range from 1% to 68% between the $2^\circ \times 2.5^\circ$ resolution and $0.5^\circ \times 0.667^\circ$ resolution simulations. This range of differences illustrates the extent of the resolution error for the coarse resolution global model.

4.2. Aggregation Error

[31] Due to the scarcity of observations, we assume uniform emission changes for a broad region instead of letting emissions be adjusted heterogeneously. This introduces aggregation error in the top-down emissions. Previous studies have quantified aggregation error for top-down constraints on other species, such as CO, but not for BC. For example, *Kopacz et al*. [2009] compared CO inversions over Asia using the adjoint inversion method with the aggregated inversion of *Heald et al*. [2004]. Without a spatially comprehensive data set of BC observations, we cannot quantify or remove the aggregation error. In this section, we discuss the potential impact of aggregation error based on model sensitivity simulations. In the sensitivity simulation, we kept the total emissions for each of the five regions (Figure 2) as the same as the bottom-up inventory but removed the spatial heterogeneity of emissions within each region by distributing the regional total emissions equally over the grid boxes. We used F_{agg} to denote the ratio of simulated BC concentrations at individual sites between the sensitivity and standard simulation (section 2). F_{agg} is 1.9, 0.9, 1.9, 2.3, and 1.0 at the LFS, TYS, GLS, MY, and CM, respectively. Comparison of F_{agg} among the sites indicates that the CM and TYS sites are subject to smaller aggregation error than the other three sites. It should be emphasized that F_{agg} is derived using an unrealistic scenario of regional homogeneous emissions, and consequently, it is quite large in value. As a result, F_{agg} cannot be taken literally as aggregation error, although it can be used to compare aggregation error across different sites.

4.3. Emission Estimate

[32] The focus of this study is to identify and quantify the representativeness error and model error in top-down BC emission estimates using observations with different temporal resolutions. The goal is to derive a top-down BC emission estimate over China in which the representativeness error and the model error are largely reduced. In order to derive the top-down emission estimate for different regions in China, we assume that the emission bias derived at the

Table 3. Comparison of the Bottom-Up [*Zhang et al*., 2009] and Top-Down BC Emissions Derived in This Study

Region[a] Represented by sites[b]	NEC LFS	CSC TYS	CC GLS	NCP MY	YRD CM	ORC -	China Total -
Bottom-up emissions (Tg/yr)	0.20	0.63	0.07	0.26	0.24	0.41	1.81
Estimated emission bias[c]	+27%	+36%	−74%	−2%	+1%	-	−0.5%
Top-down emissions (Tg/yr)	0.16	0.46	0.27	0.26	0.24	0.41	1.80
Overall uncertainty of top-down emissions	44%	53%	42%	10%	18%	37%	36%

[a]NEC = North East China, CSC = Center South China, CC = Center China, NCP = North China Plain, YRD = Yangtze River Delta, ORC = Other regions of China.
[b]LFS = Longfengshan, TYS = Taiyangshan, GLS = Gaolanshan, MY = Miyun, CM = Chongming.
[c]Positive value means overestimation; negative value means underestimation.

five rural sites can be used to represent the mean bias of regional emissions over the five regions they are located in (Figure 2). The top-down emission estimate for NCP and YRD regions is based on hourly observations at MY and CM after excluding the pollution cases and wet deposition cases. As hourly observations were not available at the other sites, the top-down emission estimate for NEC, CSC, and CC regions is based on monthly observations at LFS, TYS, and GLS, respectively. As we do not have observations to constrain emissions from ORC, the bottom-up BC emissions over ORC are used in the summation of the national total top-down emissions.

[33] As shown in Table 3, our final evaluation of BC emissions by region is that the bottom-up inventory of *Zhang et al*. [2009] overestimated BC emissions over YRD, NEC, and CSC by 1%, 27%, and 36% but underestimated emissions over CC and NCP, regions by 74% and 2%, respectively. Our estimate of China BC emissions is 1.80 Tg in 2006, which is very close (0.5% lower) to that of *Zhang et al*. [2009]. The bias of the bottom-up emission inventory is different in different regions. For the two regions where we used hourly observations (NCP and YRD), our top-down estimates were very close to the inventory (within ±2%). Over NEC and CSC, the bottom-up inventory has high biases of around 30%. The only region with large emission bias is CC, in which the inventory has underestimated emissions by 74%.

[34] Sensitivity simulations using the top-down emissions were conducted for January, April, July, and October. According to Table 3, top-down BC emissions used in the sensitivity simulations are 79%, 74%, 380%, 102%, and 99% of the original bottom-up emissions of *Zhang et al*. [2009] over NEC, CSC, CC, NCP, and YRD, respectively. The simulated concentrations at the corresponding sites are about 83%, 80%, 340%, 109%, and 100% of the original model results, respectively. The relative changes of BC concentrations are within 10% of those in emissions, further confirming our linearity assumption.

[35] The overall uncertainties shown in Table 3 are calculated as the RSS error (root of sum of squared error) of various components. There are four components of uncertainties considered when the continuous hourly observations were used at MY and CM: measurement uncertainty (10%); standard deviation of the correlation slope between modeled and observed hourly BC (2%), uncertainty in excluding the pollution cases (2% at MY and 13% at CM), and uncertainty in excluding the wet removal cases (1% at MY and 8% at CM). For the other regions with only monthly mean observations at their representative sites, the overall uncertainty includes the measurement uncertainty (10%), the standard deviation of the correlation slope (14% at LFS, 32% at TYS, and 5% at GLS), and a third term which reflects the representativeness error of using monthly mean instead of hourly observations as emission constraints. The representativeness error is taken as 41%, which is the largest difference between hourly derived and monthly derived top-down emissions at MY and CM with both hourly and monthly observations. The calculated overall uncertainties in emission estimates are 44%, 53%, 42%, 10%, and 18% for NEC, CSC, CC, NCP, and YRD, respectively. We also assume that the uncertainty for ORC is the mean uncertainty (RMS error) of that in other regions (37%). Based on the emission estimates and uncertainties in each region, the uncertainty of the top-down emission estimate for the whole China is ±36% (±0.65 Tg). This uncertainty is much smaller than that of the bottom-up inventory (±208%).

[36] It should be mentioned that our top-down emissions and the uncertainties presented above do not consider the following three issues. First, due to the lack of observations, we did not have top-down emission estimates for the ORC region which contributes 22% of China's total BC emissions according to the inventory of *Zhang et al*. [2009]. Second, our top-down emissions are quoted for 2006 to be consistent with the bottom-up inventory used in the model and observations taken at the three monthly mean sites, but the emission estimates at MY and CM are based on 2010 observations and meteorology. Two studies were found to have estimated the change of China's BC emissions from 2006 to 2010 [*Qin and Xie*, 2012; *Wang et al*., 2012], but their results were contradictory. *Qin and Xie* [2012] indicated that the overall BC emissions in China increased by about 4% per year during 2006–2009, while *Wang et al*. [2012] suggested that the emissions decreased by about 3% per year during the same period. Both studies attributed the increase/decrease mostly to the regions other than NCP or YRD, such as Central China for which our top-down estimates also gave the largest uncertainty. The third issue is the aggregation error. As discussed in section 4.2, the aggregation error may differ by sites/regions, but we cannot provide a quantitative estimate of this error in the top-down estimates due to the limitation in observations. Therefore, aggregation error is not included in the uncertainty of our top-down estimates.

[37] For the MY and CM sites with both BC and CO measurements, we can evaluate the bottom-up emission inventory by economic sectors using the BC-CO correlation slope. Emission ratios of BC and CO can vary largely from different sectors. As shown in Table 4, observed BC-CO slopes are

Table 4. BC/CO Emission Ratios of Different Sectors From *Zhang et al*. [2009] in NCP and YRD Together With BC-CO Correlation Slopes of Measured and Simulated Results, Unit: $\mu g\, m^{-3}$/ppbv

	Residential	Industry	Transport	Power[a]	Obs BC/CO	Mod BC/CO
NCP	0.0209	0.0086	0.0052	0.0141	0.0039	0.0089
YRD	0.0146	0.0062	0.0056	0.0133	0.0042	0.0074

[a]The power sector emits very little of BC and CO.

much smaller than the modeled slopes at both sites, indicating that the bottom-up inventory of *Zhang et al*. [2009] overestimated the BC/CO emission ratios over NCP and YRD regions. Residential, industry, and transportation sectors are the three major contributors to BC emissions in China. The mean BC/CO emission ratio in industry and transport sector is similar to the observed BC/CO ratio, but that in residential sector is much higher. This suggests that the overestimation of BC/CO ratio in the inventory is most likely caused by the overestimation of this ratio in residential sources. Therefore, BC emissions from the residential sector need to have a lower share in the total emissions of BC and/or a much lower BC/CO emission ratio. This is consistent with the recent bottom-up CO inventory of *Zhao et al*. [2012], which indicated that the bottom-up CO emissions had a bias of 20% over China as a whole but large uncertainty exists in residential sector. They suggested that the contribution of residential sector to overall CO emissions had decreased from 40% in 2005 to 34% in 2009 because of the increasing combustion efficiency. Therefore, the BC/CO emission ratio and presumably BC contributions in residential sector should be reduced.

4.4. Comparison With Other Studies

[38] Our top-down estimate of China BC emissions (1.80 Tg/yr in 2006) is very close to the bottom-up emission inventory of *Zhang et al*. [2009] for the same year (1.81 Tg/yr). In another top-down estimate also based on the same bottom-up inventory, *Kondo et al*. [2011b] used continuous BC measurements at a remote island (Hedo, Japan) outside China. They made a careful selection of the observations to identify which data represented the emissions from China without being significant influenced by wet removal. Their estimate of China's BC emissions was 1.92 Tg/yr, 7% larger than our top-down estimate. Although both studies used continuous hourly measurements with data screening as constraints, *Kondo et al*. [2011b] relied on one downwind site to constrain the total emissions from China, whereas we employed multiple sites inside China to give both national and regional emission estimates. Two other bottom-up emission inventories have been often used in previous studies, *Bond et al*. [2004] and *Cofala et al*. [2007]. They reported China's total emissions in 2000 of 1.36 Tg and 2.06 Tg, about 25% lower and 14% higher than our top-down estimate, respectively. Although their emission estimates are for a different year (2000), both are inside our uncertainty range (36%). Considering the regional differences, our top-down BC emissions for NEC, CSC, CC, NCP, and YRD are 11%, 1%, 390%, 50%, and 88% higher than those reported in *Bond et al*. [2004] by region, respectively.

[39] Our top-down analysis suggests that national total BC emissions over China are close to the bottom-up inventory of *Zhang et al*. [2009], while regional emissions are generally within 36% of that inventory except for CSC. Many previous modeling studies indicated BC emissions in China have been largely underestimated by at least 50% [*Koch et al*., 2009; *Wang et al*., 2011a; *Park et al*., 2005]. These studies relied on measurements with coarse temporal resolution (yearly or monthly mean data) to quantify model biases, and some of them even included urban observations along with rural ones. As illustrated before, some of the measurements may not be appropriate to represent the average BC emissions in a region. Moreover, the models used in these studies were also with coarser resolutions than our model, often coarser than $2^\circ \times 2.5^\circ$, which made their comparisons more subject to the representativeness error of observations for a large grid. The limitation of both measurement data and models are likely to introduce biases in the top-down estimates of Chinese BC emissions. One study using hourly measurements [*Hakami et al*., 2005] found that the inventory of *Street et al*. [2003a] (0.91 Tg/yr) overestimated BC emissions by 80% over Southeastern China but underestimated BC emissions by 40% and 10% in Northeastern China and Beijing, respectively. Considering the large difference between the inventory of *Street et al*. [2003a] and *Zhang et al*. [2009], the results from *Hakami et al*. [2005] are not consistent with the above-mentioned studies or our estimate. Since their analysis was based on BC observations outside China, the influence of transport and deposition can significantly affect their results. A more recent top-down analysis by *Fu et al*. [2012], which used the same nested-grid GEOS-Chem model as our study, concluded that all bottom-up inventories have underestimated Chinese BC emissions by at least 60%. Their emission estimate was 3.05 ± 0.78 Tg/yr for China, about 69% larger than our estimate (1.80 ± 0.65 Tg/yr). They used monthly mean data at several selected Chinese rural sites (including LFS, GLS, and TYS), which are subject to larger representativeness errors than hourly observations. They did not exclude the impact of the model's resolution or wet removal on their top-down emission estimates. Furthermore, their estimate was calculated based on one regression relationship between model results and observations at all the observation sites in China, which did not consider the regional differences. To summarize, previous analyses reporting that BC emissions were largely underestimated throughout China did not account for representativeness errors caused by site location, temporal resolution of measurements, and the model's spatial resolution. Based on the comparison between monthly and hourly data as model constraints, we have shown that temporal resolution causes significant biases in the top-down emissions.

5. Conclusion and Implication

[40] We simulated BC in China using a 3-D chemical transport model and estimated the BC emissions by comparing the modeled concentrations with surface observations at

two continuous and three discontinuous rural sites (either mountain or island) with measurements lasting for at least three seasons. For the two continuous sites (MY and CM), we found that the inferred model bias using hourly observations were very different from that inferred from monthly mean observations. For example, the model bias at CM changed from +42% (monthly observations) to −22% (hourly observations). We argue that hourly observations should be a better choice than monthly mean observations to derive the top-down emissions of BC because arithmetic mean observations averaged at monthly time steps can be greatly influenced by outliers or missing data. Our further analysis pointed out that there are intrinsic biases with the grid-based models in simulating high pollution events and wet removal processes and these model biases should not be translated as the emission biases. After excluding those data heavily influenced by the two types of model process biases, the mean difference between modeled and observed BC concentrations decreased from −11% to −2% at MY and from −22% to +1% at CM. Back trajectories analysis was used to define the regions which can be represented by these sites. Based on these analyses, our study concludes that the bottom-up inventory of *Zhang et al*. [2009] has overestimated regional BC emissions by 27%, 36%, and 1% over NEC, CSC, and YRD but underestimated by 74% and 2% over CC and NCP, respectively. The larger uncertainties assigned to the top-down emission estimates over NEC, CSC, and CC reflect the potential bias resulting from the use of monthly mean observations as observational constraints. Our final top-down estimate of China BC emissions is 1.80 ± 0.65 Tg/yr.

[41] Our top-down BC emission estimate is very close to the bottom-up inventory of *Zhang et al*. [2009] and within 35% difference compared with the inventory of *Bond et al*. [2004] and *Cofala et al*. [2007]. Many previous modeling studies have indicated that BC emissions in China were highly underestimated by bottom-up inventories. Most of them did not account for representativeness errors caused by site location, temporal resolution of measurements, and the model's spatial resolution. A majority of previous studies used either yearly or monthly mean observations from discontinuous measurements or mixed urban observations with rural observations, which could not represent the regional emissions and were not appropriate to be compared with model simulations, especially when they used a model with a coarse spatial resolution. Difficulties in quantifying Chinese emissions of BC may also affect other model studies of BC. For example, in order to reproduce observed concentrations in the Arctic, *Wang et al*. [2011a] increased the BC emissions in China by up to 100%. Our estimate indicates that BC emission inventories in China may not be as inaccurate as previous studies suggested, though continued careful analysis of both the representativeness of observations and the model deficiencies is needed.

[42] This study has two clear limitations that need to be solved in the future. First, we only have continuous observations from two surface sites. Monthly mean observations from the other three rural sites may cause quite large uncertainty in our top-down emission estimate. Furthermore, we used observations from one site to infer emissions from a large region (Figure 2). This introduces the representativeness error and aggregation error. We reduced the representativeness error by using back trajectories to define the regions and by excluding plume episodes not reflecting typical emission conditions. By assuming a uniform emission adjustment per region instead of letting emissions be adjusted heterogeneously, our top-down analysis is still subject to aggregation error, which can be large for some regions as discussed in section 4.2. More rural observations with higher temporal resolution are needed across different spatial regions of China. Second, although our analysis indicated that there were biases in the model's wet removal process, we cannot quantify or correct for this bias. Future studies will be needed to conduct more continuous BC measurements in China both at surface sites and through aircraft measurements.

[43] **Acknowledgments.** This research was supported by the International Science & Technology Cooperation Program of China (2010DFA21300) and the CAS Strategic Priority Research Program (Grant XDA05100403). Y. Wang acknowledges additional support from the Ministry of Education of China (NCET-11-0280). Y. Kondo and M. Irwin were supported by the Ministry of Education, Culture, Sports, Science, and Technology (MEXT) of Japan, the strategic international cooperative program of the Japan Science and Technology Agency (JST), the global environment research fund of the Japanese Ministry of the Environment (A-0803 and A-1101), and the GRENE Arctic Climate Change Research Project. Trace gas measurements at the Miyun site were supported by the Harvard University Center for the Environment, Harvard Smeltzer Fund, and an anonymous private foundation, and data analyses were supported in part by a National Science Foundation grant ATM-0635548.

References

Andreae, M. O., O. Schmid, H. Yang, D. Chand, J. Z. Yu, L. M. Zeng, and Y. H. Zhang (2008), Optical properties and chemical composition of the atmospheric aerosol in urban Guangzhou, China, *Atmos. Environ.*, *42*(25), 6335–6350, doi:10.1016/j.atmosenv.2008.01.030.

Bey, I., D. J. Jacob, R. M. Yantosca, J. A. Logan, B. Field, A. M. Fiore, Q. Li, H. Liu, L. J. Mickley, and M. Schultz (2001), Global modeling of tropospheric chemistry with assimilated meteorology: Model description and evaluation, *J. Geophys. Res.*, *106*, 23,073–23,095.

Bian, H., M. Chin, S. R. Kawa, H. Yu, T. Diehl, and T. Kucsera (2010), Multiscale carbon monoxide and aerosol correlations from satellite measurements and the GOCART model: Implication for emissions and atmospheric evolution, *J. Geophys. Res.*, *115*, D07302, doi:10.1029/2009JD012781.

Bond, T. C., D. G. Streets, K. F. Yarber, S. M. Nelson, J. H. Woo, and Z. Klimont (2004), A technology-based global inventory of black and organic carbon emissions from combustion, *J. Geophys. Res.*, *109*, D14203, doi:10.1029/2003JD003697.

Cao, G. L., X. Y. Zhang, and F. C. Zheng (2006), Inventory of black carbon and organic carbon emissions from China, *Atmos. Environ.*, *40*(34), 6516–6527.

Carmichael, G. R., et al. (2003), Regional-scale chemical transport modeling in support of the analysis of observations obtained during the TRACE-P experiment, *J. Geophys. Res.*, *108*(D21), 8823, doi:10.1029/2002JD003117.

Chen, D., Y. Wang, M. B. McElroy, K. He, R. M. Yantosca, and P. Le Sager (2009), Regional CO pollution and export in China simulated by the high-resolution nested-grid GEOS-Chem model, *Atmos. Chem. Phys.*, *9*, 3825–3839.

Chin, M., P. Ginoux, S. Kinne, O. Torres, B. Holben, B. N. Duncan, R. V. Martin, J. A. Logan, A. Higurashi, and T. Nakajima (2002), Tropospheric aerosol optical thickness from the GOCART model and comparisons with satellite and sunphotometer measurements, *J. Atmos. Sci.*, *59*, 461–483.

Cofala, J., M. Amann, Z. Klimont, K. Kupianien, and L. Hoglund-lsaksson (2007), Scenarios of global anthropogenic emissions of air pollutants and methane until 2030, *Atmos. Env.*, *41*, 38, 8486–8499.

Cooke, W. F., C. Liousse, H. Cachier, and J. Feichter (1999), Construction of a $1° \times 1°$ fossil fuel emission data set for carbonaceous aerosol and implementation and radiative impact in the ECHAM-4 model, *J. Geophys. Res.*, *104*, 22,137–22,162.

Croft, B., U. Lohmann, and K. von Salzen (2005), Black carbon ageing in the Canadian Centre for Climate modelling and analysis atmospheric general circulation model, *Atmos. Chem. Phys.*, *5*, 1931–1949.

Dachs, J., and Eisenreich, S. J. (2000), Adsorption onto aerosol soot carbon dominates gas-particle partitioning of polycyclic aromatic hydrocarbons, *Environ. Sci. Technol.*, *34*, 17, 3690–3697.

Feng, J. (2007), A 3-mode parameterization of below-cloud scavenging of aerosols for use in 625 atmospheric dispersion models, *Atmos. Environ.*, *41*, 6808–6822, 626, doi:10.1016/j.atmosenv.2007.04.046.

Fu, T.-M., et al. (2012), Carbonaceous aerosols in China: Top-down constraints on primary sources and estimation of secondary contribution, *Atmos. Chem. Phys.*, *12*, 2725–2746.

Gilardoni, S., E. Vignati, and J. Wilson (2011), Using measurements for evaluation of black carbon modeling, *Atmos. Chem. Phys.*, *11*, 439–455.

Hakami, A., D. K. Henze, J. H. Seinfeld, T. Chai, Y. Tang, G. R. Carmichael, and A. Sandu (2005), Adjoint inverse modeling of black carbon during the Asian Pacific Regional Aerosol Characterization Experiment, *J. Geophys. Res.*, *110*, D14301, doi:10.1029/2004JD005671.

Han, S., et al. (2009), Temporal variations of elemental carbon in Beijing, *J. Geophys. Res.*, *114*, D23202, doi:10.1029/2009JD012027.

Heald, C. L., D. J. Jacob, D. B. A. Jones, P. I. Palmer, J. A. Logan, D. G. Streets, G. W. Sachse, J. C. Gille, R. N. Hoffman, and T. Nehrkorn (2004), Comparative inverse analysis of satellite (MOPITT) and aircraft (TRACE-P) observations to estimate Asian sources of carbon monoxide, *J. Geophys. Res.*, *109*, D23306, doi:10.1029/2004JD005185.

Hirsch, R. M., and E. J. Gilroy (1984), Methods of fitting a straight-line to data- Examples in water resources, *Water Resour. Bull.*, *20*(5), 705–711.

Hu, Y., M. T. Odman, and A. G. Russell (2009), Top-down analysis of the elemental carbon emissions inventory in the United States by inverse modeling using Community Multiscale Air Quality model with decoupled direct method (CMAQ-DDM), *J. Geophys. Res.*, *114*, D24302, doi:10.1029/2009JD011987.

Huang, Y., S. Wu, M. K. Dubey, and N. H. F. French (2012), Impact of aging mechanism on model simulated carbonaceous aerosols, *Atmos. Chem. Phys. Discuss.*, *12*, 28993–29023, doi:10.5194/acpd-12-28993-2012.

Jacobson, M. Z. (2001), Strong radiative heating due to the mixing state of black carbon in atmospheric aerosols, *Nature*, *409*(6821), 695–697.

Koch, D., et al. (2009), Evaluation of black carbon estimations in global aerosol models, *Atmos. Chem. Phys.*, *9*, 9001–9026, doi:10.5194/acp-9-9001-2009.

Kondo, Y., et al. (2009), Stabilization of the mass absorption cross section of black carbon for filter-based absorption photometry by the use of a heated inlet, *Aerosol. Sci. Tech.*, *43*, (8), 741–756.

Kondo, Y., L. Sahu, N. Moteki, F. Khan, N. Takegawa, X. Liu, M. Koike, and T. Miyakawa (2011a), Consistency and traceability of black carbon measurements made by laser-induced incandescence, thermal-optical transmittance, and filter-based photo-absorption techniques, *Aerosol. Sci. Technol.*, *45*, 295–312, doi:10.1080/02786826.2010.533215.

Kondo, Y., N. Oshima, M. Kajino, R. Mikami, N. Moteki, N. Takegawa, R. L. Verma, Y. Kajii, S. Kato, and A. Takami (2011b), Emissions of black carbon in East Asia estimated from observations at a remote site in the East China Sea, *J. Geophys. Res.*, *116*, D16201, doi:10.1029/2011JD015637.

Kopacz, M., D. J. Jacob, D. K. Henze, C. L. Heald, D. G. Streets, and Q. Zhang (2009), Comparison of adjoint and analytical Bayesian inversion methods for constraining Asian sources of carbon monoxide using satellite (MOPITT) measurements of CO columns, *J. Geophys. Res.*, *114*, D04305, doi:10.1029/2007JD009264.

Lei, Y., Zhang, Q., He, K. B., and Streets, D. G. (2011), Primary anthropogenic aerosol emission trends for China, 1990–2005, *Atmos. Chem. Phys.*, *11*, 931–954.

Li, C., L. T. Marufu, R. R. Dickerson, Z. Li, T. Wen, Y. Wang, P. Wang, H. Chen, and J. W. Stehr (2007), In situ measurements of trace gases and aerosol optical properties at a rural site in northern China during East Asian Study of tropospheric aerosols: An International Regional Experiment 2005, *J. Geophys. Res.*, *112*, D22S04, doi:10.1029/2006JD007592.

Liu, H. Y., D. J. Jacob, I. Bey, and R. M. Yantosca (2001), Constraints from Pb-210 and Be-7 on wet deposition and transport in a global three-dimensional chemical tracer model driven by assimilated meteorological fields, *J. Geophys. Res. Atmos.*, *106*, 12109–12128.

Liu, S., and X. Liang (2010), Observed diurnal cycle climatology of planetary boundary layer height, *J. Climate*, *23*, 5790–5809, doi:10.1175/2010JCLI3552.1.

Lu, Z., Q. Zhang, and D. G. Streets (2011), Sulfur dioxide and primary carbonaceous aerosol emissions in China and India, 1996–2010, *Atmos. Chem. Phys.*, *11*, 9839–9864.

Miyazaki, Y., Y. Kondo, L. K. Sahu, J. Imaru, N. Fukushima, and M. Kano (2008), Performance of a newly designed continuous soot monitoring system (COSMOS), *J. Environ. Monitor*, *10*(10), 1195–1201.

Pan, X. L., et al. (2011), Correlation of black carbon aerosol and carbon monoxide in the high-altitude environment of Mt. Huang in Eastern China, *Atmos. Chem. Phys.*, *11*, 9735–9747.

Park, R. J., et al. (2005), Export efficiency of black carbon aerosol in continental outflow: Global implications, *J. Geophys. Res.*, *110*, D11205, doi:10.1029/2004JD005432.

Park, R. J., D. J. Jacob, M. Chin, and R. V. Martin (2003), Sources of carbonaceous aerosols over the United States and implications for natural visibility, *J. Geophys. Res.*, *108*(D12), 4355, doi:10.1029/2002JD003190.

Park, R. J., et al. (2010), A contribution of brown carbon aerosol to the aerosol light absorption and its radiative forcing in East Asia, *Atmos. Environ.*, *44*, 1414–1421.

Qin, Y., and S. D. Xie (2012), Spatial and temporal variation of anthropogenic black carbon emissions in China for the period 1980–2009, *Atmos. Chem. Phys.*, *12*, 4825–4841.

Ramanathan, V., and G. Carmichael (2008), Global and regional climate changes due to black carbon, *Nat. Geosci.*, *1*(4), 221–227.

Schaap, M., R. P. Otjes, and E. P. Weijers (2011), Illustrating the benefit of using hourly monitoring data on secondary inorganic aerosol and its precursors for model evaluation, *Atmos. Chem. Phys.*, *11*, 11041–11053.

Streets, D. G., S. Gupta, S. T. Waldhoff, M. Q. Wang, T. C. Bond, and Y. Y. Bo (2001), Black carbon emissions in China, *Atmos. Environ.*, *35*(25), 4281–4296, doi:10.1016/S1352-2310(01)00179-0.

Streets, D. G., et al. (2003a), An inventory of gaseous and primary aerosol emissions in Asia in the year 2000, *J. Geophys. Res.*, *108*(D21), 8809, doi:10.1029/2002JD003093.

Streets, D. G., K. F. Yarber, J. H. Woo, and G. R. Carmichael (2003b), Biomass burning in Asia: Annual and seasonal estimates and atmospheric emissions, *Global Biogeochem. Cycles*, *17*(4), 1099, doi:10.1029/2003GB002040.

Streets, D. G., Q. Zhang, L. Wang, K. He, J. Hao, Y. Wu, Y. Tang, and G. R. Carmichael (2006), Revisiting China's CO emissions after TRACE-P: Synthesis of inventories, atmospheric modeling, and observations, *J. Geophys. Res.*, *111*, D14306, doi:10.1029/2006JD007118.

Tanimoto, H., Y. Sawa, S. Yonemura, K. Yumimoto, H. Matsueda, I. Uno (2008), Diagnosing recent CO emissions and ozone evolution in East Asia using coordinated surface observations, adjoint inverse modeling, and MOPITT satellite data. *Atmos. Chem. Phys.*, *8*, 3867–3880.

van der Werf, G. R., et al. (2010), Global fire emissions and the contribution of deforestation, savanna, forest, agricultural, and peat fires (1997–2009), *Atmos. Chem. Phys. Discuss*, *10*, 16153–16203.

Verma, R. L., Y. Kondo, N. Oshima, H. Matsui, K. Kita, L. K. Sahu, S. Kato, Y. Kajii, A. Takami, and T. Miyakawa (2011), Seasonal variations of the transport of black carbon and carbon monoxide from the Asian continent to the western Pacific in the boundary layer, *J. Geophys. Res.*, *116*, D21307, doi:10.1029/2011JD015830.

Wang, Y. X., M. B. McElroy, D. J. Jacob, and R. M. Yantosca (2004), A nested grid formulation for chemical transport over Asia: Applications to CO, *J. Geophys. Res.*, *109*, D22307, doi:10.1029/2004JD005237.

Wang, Y., M. B. McElroy, J. W. Munger, J. Hao, H. Ma, C. P. Nielsen, and Y. Chen (2008), Variations of O-3 and CO in summertime at a rural site near Beijing, *Atmos. Chem. Phys.*, *8*(21), 6355–6363.

Wang, Y., J. Hao, M. B. McElroy, J. W. Munger, H. Ma, D. Chen, and C. P. Nielsen (2009), Ozone air quality during the 2008 Beijing Olympics: Effectiveness of emission restrictions, *Atmos. Chem. Phys.*, *9*, 14, 5237–5251.

Wang, Y., J. W. Munger, S. Xu, M. B. McElroy, J. Hao, C. P. Nielsen, and H. Ma (2010), CO_2 and its correlation with CO at a rural site near Beijing: Implications for combustion efficiency in China, *Atmos. Chem. Phys.*, *10*(18), 8881–8897.

Wang, Q., et al. (2011a), Sources of carbonaceous aerosols and deposited black carbon in the Arctic in winter-spring: Implications for radiative forcing, *Atmos. Chem. Phys.*, *11*, 12453–12473.

Wang, Y., X. Wang, Y. Kondo, M. Kajino, J. W. Munger, and J. Hao (2011b), Black carbon and its correlation with trace gases at a rural site in Beijing: Top-down constraints from ambient measurements on bottom-up emissions, *J. Geophys. Res.*, *116*, D24304, doi:10.1029/2011JD016575.

Wang, R., et al. (2012), Black carbon emissions in China from 1949 to 2050, *Environ. Sci. Technol. 46*, 7595–7603.

Wesely, M. L. (1989), Parameterization of surface resistances to gaseous dry deposition in regional-scale numerical-models, *Atmos. Environ.*, *23*, 1293–1304.

Zhang, X. Y., Y. Q. Wang, X. C. Zhang, W. Guo, S. L. Gong, P. Zhao, and J. L. Jin (2008), Carbonaceous aerosol composition over various regions of China during 2006, *J. Geophys. Res.*, *113*, D14111, doi:10.1029/2007JD009525.

Zhang, Q., et al. (2009), Asian emissions in 2006 for the NASA INTEX-B mission, *Atmos. Chem. Phys.*, *9*(14), 5131–5153.

Zhao, Y., C. P. Nielsen, M. B. McElroy, L. Zhang, and J. Zhang (2012), CO emissions in China: Uncertainties and implications of improved energy efficiency and emission control, *Atomos. Env.*, *49*, 103–113.

Zhou, X. H., J. Cao, T. Wang, W. S. Wu, and W. X. Wang (2009), Measurement of black carbon aerosols near two Chinese megacities and the implications for improving emission inventories, *Atmos. Environ.*, *43*(25), 3918–3924, doi:10.1016/j.atmosenv.2009.04.062.